

Unveiling hadronic resonance dynamics at LHC energies: insights from EPOS4

Vikash Sumberia^{*1}, Dukhishyam Mallick^{†2}, Sanjeev Singh Sambyal^{‡1}, and Nasir Mehdi Malik^{§1}

¹University of Jammu, J&K, India

²Université Paris-Saclay, CNRS/IN2P3, IJCLab, Orsay, France

December 9, 2024

Abstract

Hadronic resonances, with lifetimes of a few fm/c are key tools for studying the hadronic phase in high-energy collisions. This work investigates resonance production in pp collisions at $\sqrt{s} = 13.6$ TeV and in Pb–Pb collisions at $\sqrt{s_{NN}} = 5.36$ TeV using EPOS4 model. It has a unique capability to switch the Ultra-relativistic Quantum Molecular Dynamics (UrQMD) ON and OFF, allowing the study of final-state hadronic interactions in the hadronic phase. We discuss studies primarily focused on hadronic resonances, along with the production of other non-strange and strange hadrons, in the context of effects such as rescattering, regeneration, baryon-to-meson production, and strangeness enhancement, using transverse momentum (p_T) spectra and particle ratios.

Rescattering and strangeness effect is found to play an important role at low p_T , whereas baryon-to-meson ratios dominate at intermediate p_T . Additionally, a strong mass-dependent radial flow is observed in the most central Pb–Pb collisions. The average p_T scaled with the reduced hadron mass (i.e., the mass divided by the number of valence quarks) is examined, revealing a deviation from a linear trend for short-lived resonances. By analyzing the yield ratios of short-lived resonances to stable hadrons in pp and Pb–Pb collisions, we estimate the time duration (τ) of the hadronic phase as a function of average charged multiplicity. The results show that τ increases with increasing multiplicity and system size, exhibiting a nonzero value in high-multiplicity pp collisions. Proton (p), strange (Λ) and multi-strange (Ξ ,

Ω) baryons production in the most central Pb–Pb collisions is influenced by competing processes of strangeness enhancement and baryon-antibaryon annihilation. Comparing these findings with measurements at LHC energies offers valuable insights into the underlying dynamics of the hadronic phase and their production dynamics.

1 Introduction

High-energy heavy-ion (AA) collisions offer a unique opportunity to study the properties of the Quark-Gluon Plasma (QGP), a deconfined state of quarks and gluons, formed under extreme conditions of temperature and/or energy density [1]. As the dense medium created in these collisions evolves and cools, it eventually reaches a point where quarks and gluons recombine into hadrons, resulting in a hadron resonance gas (HRG). The study of the production yield of hadronic resonances offers valuable insight into the properties of the hadronic phase, which exists between chemical freeze-out (when inelastic collisions stop) and kinetic freeze-out (when elastic collisions stop) [2]. The decay products of resonances can undergo regeneration or rescattering through elastic or pseudo-elastic interactions, which involve scattering via intermediate resonance states. These processes can modify the original yields of resonances produced before chemical freeze-out. In the rescattering process, if at least one decay product interacts elastically with other hadrons, the four-momentum information of the parent resonance is altered. This alteration prevents accurate reconstruction of the resonance, and thus the parent resonance particle is said to be lost. Conversely, regeneration occurs when pseudo-elastic interactions among hadrons recreate the parent resonance, leading to an in-

^{*}Corresponding author: vikash.sumberia@cern.ch

[†]Corresponding author: dukhishyam.mallick@cern.ch

[‡]sanjeev.singh.sambyal@cern.ch

[§]nasir.mehdi.malik@cern.ch

crease in the reconstructed yield compared to the original resonance yield. The dominance of rescattering or regeneration can be explored by analyzing the yield ratios of resonances to longer-lived hadrons with similar quark content as a function of system size. To investigate hadronic resonance production and their interactions, various resonances with different lifetimes, valence quark flavors, masses, and spins have been studied at LHC [3, 4, 5, 5, 6, 7, 8] and RHIC [9, 10, 11] energies. These studies provide insight into the dynamics of the hadronic phase and the modification of resonance yields in different collision systems.

Recent measurements show that the yields of short-lived resonances, such as the $\rho(770)^0$ (1.335 fm/c) and $K^*(892)^0$ (4.16 fm/c), are significantly modified in the hadronic phase compared to longer-lived resonances like the $\phi(1020)$ meson (46.26 fm/c). This is attributed to the fact that short-lived resonances decay within the hadronic medium, where processes such as rescattering and regeneration affect their yields. In contrast, longer-lived resonances typically decay after the hadronic phase, when the medium has expanded sufficiently and the interactions are minimal, resulting in a little or no yield modification [3, 4, 6]. For baryonic resonances, such as the $\Sigma(1385)^\pm$ (5.0–5.5 fm/c) and $\Lambda(1520)$ (12.54 fm/c), Pb–Pb collision studies have shown yield modification for $\Lambda(1520)$ but not for $\Sigma(1385)^\pm$, despite the latter having a shorter lifetime [12]. Interestingly, such studies in small collision systems indicate no significant yield modification for these resonances [6].

Recent such measurements in high-multiplicity small collisions show behavior similar to that observed in heavy-ion collisions. The $K^*(892)^0$ measurement shows a decreasing trend in yield with multiplicity, indicating the presence of a nonzero hadronic phase duration in high-multiplicity pp and p–Pb collisions, as reported in Ref. [13, 14]. To understand the dynamics of the modification of resonance production in the hadronic phase, various approaches have been carried out. One such approach is the use of the transport AMPT model that simulates the time evolution of the system through microscopic interactions between particles. This model accounts for processes such as scattering, regeneration, and decay of resonances during the hadronic phase [15]. Another approach involves the HRG model in partial chemical equilibrium (PCE). This model describes the dynamics of particle yields and reactions in the hadronic phase, capturing the interplay between resonance decay, regeneration, and freeze-out conditions [16]. Additionally, the SMASH model (Simulating Many Accelerated Strongly-interacting Hadrons) is a hadronic transport model designed to simulate the non-equilibrium dynam-

ics of hadronic systems. It accounts the hydrodynamic description with the SMASH as a hadronic afterburner, modeling the evolution of the system after the QGP transitions into a hadron-dominated medium [17]. The findings from experimental measurement and theoretical studies suggest that the final resonance yields are influenced not only by their lifetimes but also by additional factors, such as the duration of the hadronic phase, the interaction cross-section of decay daughters, the freeze-out temperature, and the mean free path of the resonances.

In this study, we present results of various hadrons, including hadronic resonances, at midrapidity ($|y| < 0.5$) for pp collisions at $\sqrt{s} = 13.6$ TeV and Pb–Pb collisions at $\sqrt{s_{NN}} = 5.36$ TeV using the EPOS4 with UrQMD hadronic afterburner both ON and OFF. The terms “with UrQMD” and “without UrQMD” are used interchangeably to refer to simulations with UrQMD ON and UrQMD OFF, respectively, and may appear throughout the text. The inclusion of UrQMD (Ultra-relativistic Quantum Molecular Dynamics) enables detailed modeling of the hadronic phase by simulating its effects on the system. These effects can significantly alter key observables such as transverse momentum (p_T) spectra, particle yields, and yield ratios, as well as collective phenomena like flow and particle correlations. By comparing simulations with and without UrQMD to experimental data, the influence of the hadronic phase on resonance production has been explored. The study also examines how strangeness enhancement and baryon-to-meson ratios influence the production of hadronic resonances and multi-strange hadrons. This comparison provides valuable insights into the dynamics of the hadronic phase and its impact on final-state observables. The highest energies and finer high-multiplicity events in small systems are chosen to improve upon previous studies [18, 19] and to offer opportunities for future comparisons with experimental measurements. Experimentally, hadronic resonances are reconstructed using the invariant-mass technique via the addition of 4-momenta of their decay daughters. The longer-lived decay daughters, such as charged pions, charged kaons, and (anti)protons, reach the detectors and are often identified through measurements of energy loss (dE/dx) in a Time Projection Chamber (TPC) and / or velocity in a Time-of-Flight (TOF) detector. The weakly decaying daughters, such as K_S^0 , Λ , Ξ and Ω can be selected based on their decay topologies, which puts further constraints. For this study, 5 million events were generated for pp collisions, both with and without UrQMD, while 1.5 million events were generated for Pb–Pb collisions under the same conditions. The events are divided into various multiplicity classes based on the

number of charged particles present within the pseudorapidity ranges $-3.7 < \eta < -1.7$ and $2.8 < \eta < 5.1$. This method follows an approach similar to that used by the ALICE experiment for pp and Pb–Pb collisions in Run 2 studies.

Particles are selected from the generated data according to their unique EPOS IDs, with weak decays disabled to ensure that only primary particles contribute to the final yield calculations. After selecting resonances based on their unique EPOS IDs, they are flagged as either reconstructible or non-reconstructible. When a resonance decays, the EPOS4 model tracks its decay daughters. If any of the decay daughters undergo elastic interactions that alter their momenta, the parent resonance is flagged as non-reconstructible. As a result, the resonance is not included in the final yield measurements. This ensures that only resonances whose decay daughters have not undergone significant elastic scattering are counted, following a similar approach to experimental measurements, where resonance particles are reconstructed based on the momenta and trajectories of their decay products. Table 1 lists the resonances and their properties, including decay channels, branching ratios, and lifetimes. The decay channels included in Table 1 are those commonly analyzed in experiments at LHC energies [20]. The shorthand notations provided in the table will be used to represent the resonances throughout the text.

Table 1: Properties of selected resonances, including their decay channels, branching ratios, and lifetimes in the rest frame [21].

Resonance	Shorthand	Decay Channel	Branching Ratio	Lifetime (fm/c)
$\rho(770)^0$	ρ^0	$\pi^+ + \pi^-$	1.0	1.335
$K^*(892)^0$	K^{*0}	$\pi^- + K^+$	0.67	4.16
$\phi(1020)$	ϕ	$K^+ + K^-$	0.492	46.26
$\Delta^{++}(1232)$	Δ^{++}	$\pi^+ + p$	1.0	1.69
$\Sigma(1385)^+$	Σ^{*+}	$\pi^+ + \Lambda$	0.870	5.48
$\Sigma(1385)^-$	Σ^{*-}	$\pi^- + \Lambda$	0.870	5.01
$\Lambda(1520)$	Λ^*	$K^- + p$	0.225	12.54
$\Xi(1530)^0$	Ξ^{*0}	$\pi^+ + \Xi^-$	0.67	22

The paper is organized as follows: Section 1 introduces hadronic resonances and their interactions within the hadronic gas. It also describes the event generation using the EPOS4 hydrodynamical model, along with particle selection methods and the criteria used for multiplicity and centrality estimation. Section 2 discusses the EPOS4 model, outlining its key concepts and emphasizing the major advancements and differences compared

to its predecessor, EPOS3. Section 3 presents results for various observables. Finally, Section 4 summarizes the key findings of this study.

2 EPOS4: Framework overview and key features

The EPOS4 model is a general-purpose framework designed to investigate a wide range of observables in relativistic collisions, from proton-proton to nucleus-nucleus collisions, at energies ranging from several GeV to multiple TeV per nucleon [22]. One of the key concepts underlying EPOS4 is parallel scattering, where multiple parton-parton scatterings occur simultaneously due to the extended reaction times in high-energy collisions. This is implemented using Gribov-Regge (GR) theory [23, 24, 25, 26], applying the S-matrix framework to manage multiple scatterings, which ensures the proper distribution of energy and momentum among the scatterings and the remnants of both the projectile and target. The EPOS4 model also accounts for those scenarios where the Dokshitzer-Gribov-Lipatov-Altarelli-Parisi (DGLAP) approach [25, 27, 28] becomes insufficient, particularly at small momentum fractions ($x \ll 1$), where the linear parton evolution assumed by DGLAP breaks down due to the increasing density of partons. These small- x regions, where the parton densities are very high, require the inclusion of nonlinear effects arising from gluon-gluon fusion, leading to “saturation” phenomena [29, 30, 31, 32, 33]. To address these saturation effects, the EPOS4 introduces a saturation scale that ensures proper factorization and binary scaling, which were violated in the previous the EPOS3 model [34]. With this new approach, the model also offers unique opportunity to distinguish between the primary and secondary scatterings: primary scatterings refer to instantaneous interactions involving initial nucleons and their partonic constituents at very high energies, while secondary scatterings involve interactions among the products of string decays. The model also improves on the core-corona procedure [35, 36, 37], dividing string segments based on energy loss and incorporating advanced methods to manage energy-momentum flow through freeze-out hypersurface [22]. These changes, along with a new microcanonical procedure [22] to conserve energy-momentum and flavor throughout primary and secondary interactions, mark significant improvements over the EPOS3, making the EPOS4 a more robust tool for modeling high-energy collisions.

3 Results and discussion

This section includes the p_T spectra, the p_T -differential and integrated yield ratios (including resonance-to-stable hadron ratios, baryon-to-meson ratios, and hadron yields to pion ratios), and the $\langle p_T \rangle$ as a function of system size from pp to Pb–Pb collisions at LHC energies. Additionally, the time duration of the hadronic phase is estimated for short-lived resonances. The discussion of these observables aims to provide insights into the hadronic phase. Whenever available, the results are compared to experimental data from the ALICE Collaboration.

3.1 Transverse momentum (p_T) spectra

To investigate the impact of the hadronic phase on resonance production, analyzing the shape of the p_T spectra can provide details about their production dynamics and interactions. The K^{*0} and ϕ mesons are ideal candidates for such studies due to their similar masses but significantly different lifetimes: the K^{*0} has a relatively short lifetime of approximately 4.16 fm/c, whereas the ϕ meson is long-lived, with a lifetime of about 46.2 fm/c, differing by nearly an order of magnitude. The upper panels of Fig. 1 show the p_T spectra of K^{*0} (left) and ϕ (right) from EPOS4 with UrQMD ON (solid lines) and OFF (dotted lines) for the centrality classes 0–10% and 60–80% at mid-rapidity ($|y| < 0.5$) in Pb–Pb collisions at $\sqrt{s_{NN}} = 5.36$ TeV. The lower panels represent the ratios of p_T spectra with UrQMD ON to those with UrQMD OFF. A significant difference is observed between UrQMD ON and OFF at low p_T for K^{*0} . The effect is more pronounced for central (0–10%, red lines) collisions than peripheral (60–80%, yellow lines) collisions. Similarly, the same ratios for pp collisions in the multiplicity class 0–1% (red) and 70–100% (cyan) at $\sqrt{s} = 13.6$ TeV are shown in Fig. 2. A similar suppression feature is also observed at low p_T in high multiplicity (0–1%) pp collisions for K^{*0} compared to ϕ . The observed suppression in high-multiplicity pp collisions is of a similar magnitude to that observed in peripheral Pb–Pb collisions. This is expected, as the multiplicity values in high-multiplicity pp collisions approach those reached in peripheral Pb–Pb collisions. For the most central Pb–Pb collisions, the suppression is more pronounced, supporting similar observations reported by ALICE measurements at LHC energies [13]. This suggests that, due to the short lifetime of the K^{*0} , its decay daughters undergo rescattering within the hadronic phase, particularly at low p_T in central Pb–Pb collisions and in high-multiplicity pp collisions. At high p_T and in low-multiplicity events, the ratios approach unity. In contrast, this effect is less pronounced

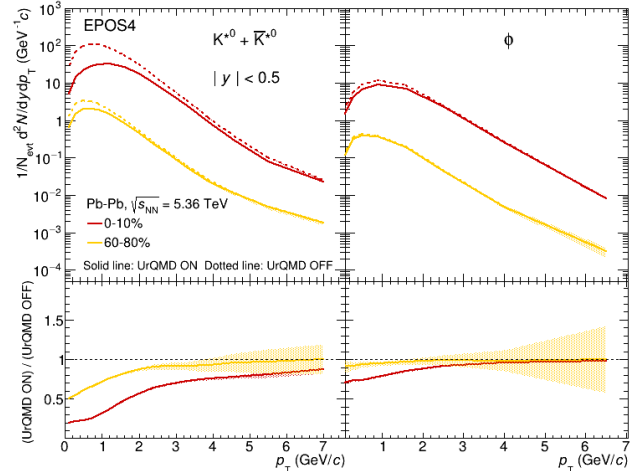


Fig. 1: Upper panel: The p_T spectra of K^{*0} and ϕ resonances in the mid-rapidity region for central (0–10%) and peripheral (60–80%) Pb–Pb collisions at $\sqrt{s_{NN}} = 5.36$ TeV with EPOS4 in UrQMD ON and UrQMD OFF tunes. The solid lines represent measurements with UrQMD ON while dotted lines represent measurements with UrQMD OFF. **Lower panel:** The p_T -differential yield ratios of K^{*0} and ϕ for UrQMD ON to UrQMD OFF tunes. The bands represent the statistical uncertainties in the measurements.

for the ϕ , as expected due to its longer lifetime. This shows that the EPOS4 model with UrQMD effectively captures the effects of the hadronic phase on resonance production.

To further investigate the effects of the hadronic phase, the ratio of p_T spectra for various hadronic resonances with lifetimes ranging from 1 to 47 fm/c with UrQMD ON and OFF is shown in Fig. 3 for central 0–10% Pb–Pb collisions at $\sqrt{s_{NN}} = 5.36$ TeV. A clear trend of suppression is observed, ordered as follows: $\rho^0 < \Delta^{++} < K^{*0} < \Sigma^{*\pm} \sim \Lambda^* < \Xi^{*0} < \phi$, with suppression increasing as the resonance lifetime decreases. However, for the Λ^* and $\Sigma^{*\pm}$ baryons, the suppression ratios appear similar despite their different lifetimes. This indicates that the lifetime of the resonance is not the only factor influencing the modification of final yields for heavier baryonic resonances in the hadronic phase.

The low- p_T (non-perturbative QCD) region of p_T spectra play important role for understanding production dynamics because the processes such as rescattering, regeneration, strangeness enhancement and baryon-to-meson can significantly influence the shape of the p_T spectra and the interactions of hadrons. The particle ratios serve as effective tools for distinguishing such processes. Specifically: (a) resonance-to-stable hadron yield ratios provide insight into the p_T distributions of hadrons with similar

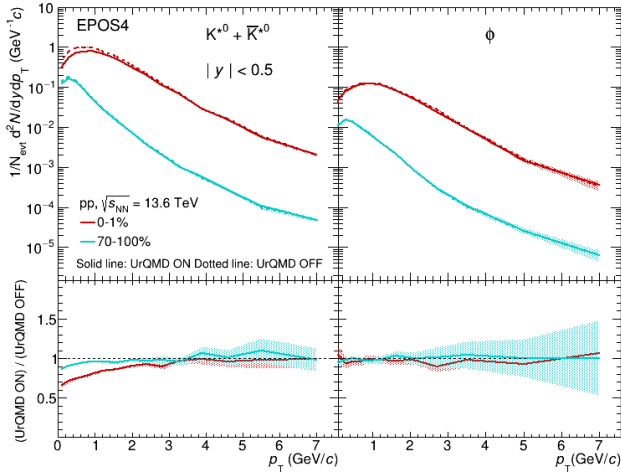


Fig. 2: Upper panel: The p_T spectra of K^{*0} and ϕ resonances in the midrapidity region for high multiplicity (0–1%) and low multiplicity (70–100%) in pp collisions at $\sqrt{s} = 13.6$ TeV with EPOS4 in UrQMD ON and UrQMD OFF tunes. The solid lines represent measurements with UrQMD ON while dotted lines represent measurements with UrQMD OFF. **Lower panel:** The p_T -differential yield ratios of K^{*0} and ϕ for UrQMD ON to UrQMD OFF tunes. The bands represent the statistical uncertainties in the measurements.

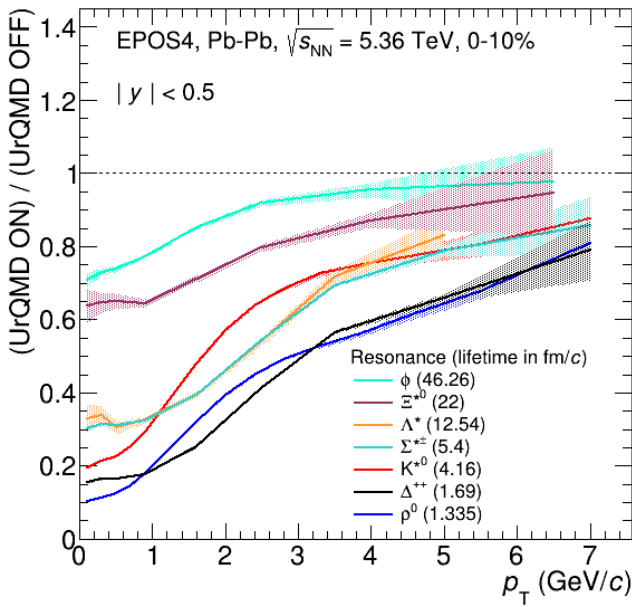


Fig. 3: The comparison of p_T -differential spectra of hadronic resonances with UrQMD to the spectra without UrQMD in central (0–10%) Pb–Pb collisions with EPOS4. The bands in the measurements represent the statistical uncertainty.

quark content but differing masses, and (b) baryon-to-meson resonance yield ratios enable the comparison of hadrons with similar masses but differing baryon numbers and quark compositions.

To quantify the p_T -dependent of the rescattering effect, in the upper panels of Fig. 4 show the comparison between p_T -differential ratios K^{*0}/K (left) and ϕ/K (right) in the central (0–10%) and peripheral (60–80%) Pb–Pb collisions at $\sqrt{s_{NN}} = 5.36$ TeV and for high multiplicity (0–1%) in pp collisions at $\sqrt{s} = 13.6$ TeV with UrQMD hadronic afterburner. The lower panels represent the p_T -differential yield ratios comparison for central and peripheral in Pb–Pb collisions to the high-multiplicity pp collisions. However, the energy in pp collisions differs from that in Pb–Pb collisions, as the resonance yield varies smoothly with charged particle multiplicity rather than depending solely on energy of the colliding system, as observed in ALICE measurements [12, 13]. Therefore, the highest multiplicity classes of pp collisions are selected as the denominator, providing a suitable baseline for comparing peripheral Pb–Pb collisions and offering further insights into their behavior. For K^{*0}/K , it is observed that the double ratio is suppressed at low- p_T , particularly in more central collisions compared to peripheral ones. This suppression is attributed to the rescattering effect, which impacts K^{*0} production but cancels out the strangeness effect due to the choice of the K^{*0}/K ratio. In contrast, for the ϕ/K ratio, no significant suppression or centrality dependence is observed. Peripheral Pb–Pb collisions and high-multiplicity pp collisions exhibit similar p_T -differential yield ratios. This similarity suggests that the hadron production mechanisms in peripheral Pb–Pb and high-multiplicity pp collisions may share common features. Similarly, p_T -differential yield ratios for various hadronic resonances are shown in Fig. 5 for centrality 0–10% (left) and peripheral 60–80% (right) in Pb–Pb collisions at $\sqrt{s_{NN}} = 5.36$ TeV. At low p_T , these ratios exhibit a specific ordering: $\Lambda^*/\Lambda < \rho^0/\pi < K^{*0}/K < \Xi^{*0}/\Xi^- \approx \Sigma^{*\pm}/\Lambda < \Delta^{**}/p < \phi/K$. Despite the longer lifetime of Λ^* , it exhibits a larger suppression compared to other short-lived resonances, a trend also observed in the p_T -integrated yield ratios for the most central Pb–Pb collisions (discussed later in Section 3.4). In contrast, for peripheral Pb–Pb collisions, the ratios approach unity, suggesting that the impact of resonance lifetimes on these ratios is minimal.

3.2 Baryon-to-meson ratios

Particle ratios, particularly baryon-to-meson ratios, are essential for understanding mass-dependent radial flow

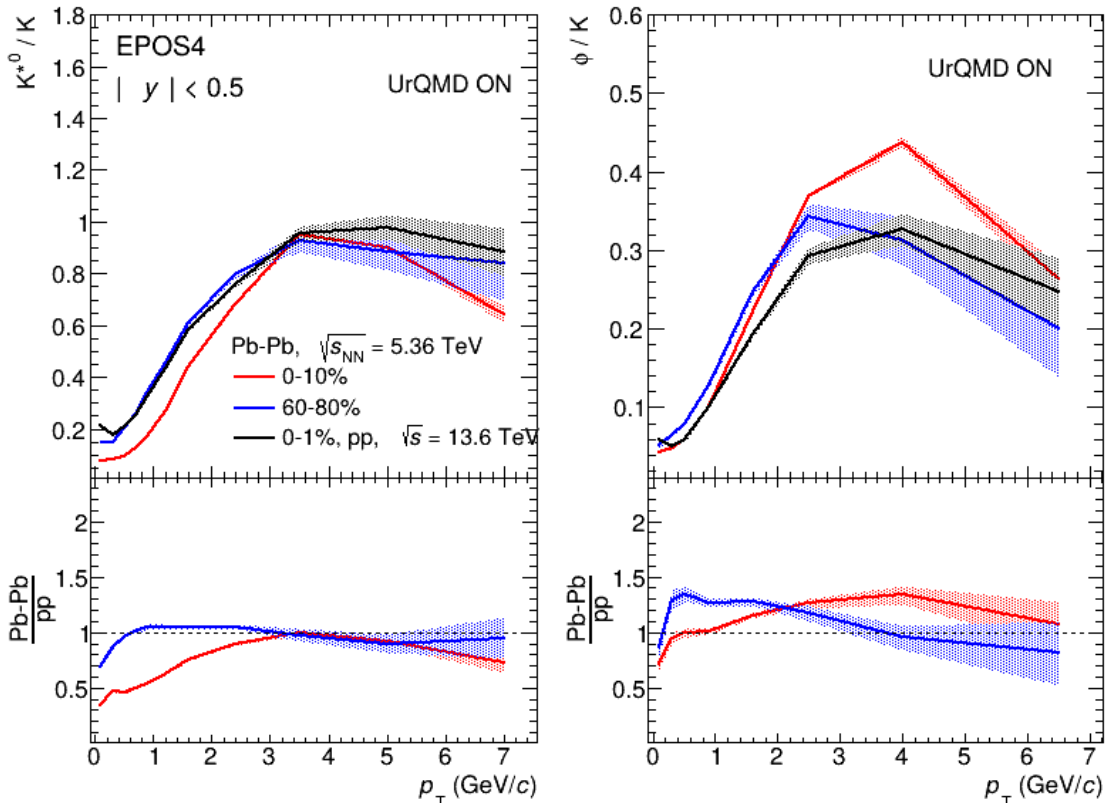


Fig. 4: Upper panel: The p_T -differential ratios K^{*0}/K (left) and ϕ/K (right) in central (0–10%) and peripheral (60–80%) Pb–Pb collisions at $\sqrt{s_{NN}} = 5.36$ TeV and in high-multiplicity (0–1%) pp collisions at $\sqrt{s} = 13.6$ TeV simulated with UrQMD. **Lower panel:** Comparison of p_T -differential ratios in central and peripheral Pb–Pb collisions to high-multiplicity pp collisions. The shaded bands represent statistical uncertainties.

and the production mechanisms of baryons and mesons. The baryon-to-meson ratios of several hadrons, including resonances such as K^{*0} , ϕ , Λ^* , and $\Sigma^{*\pm}$, are discussed using calculations from EPOS4 with and without UrQMD. The EPOS4 with UrQMD captures a clear mass-dependent enhancement at low to intermediate p_T in the ratios of baryons (Λ , Λ^* , and $\Sigma^{*\pm}$) to K_S^0 for the most central Pb–Pb collisions, as shown in Fig. 6. Similar features are seen in the ratios of p/π and Λ/K_S^0 for light-flavor hadrons in central Pb–Pb collisions, consistent with observations reported by ALICE Collaboration in Ref. [38, 39]. Moreover, the enhancement decreases, and the peak position shifts toward high- p_T region with increasing baryon masses. An alternative explanation is that the quark recombination drives baryon-to-meson enhancement. The baryon production is favored because three quarks combining to form a baryon is more probable than forming a meson through a quark-antiquark pair [40]. To distinguish whether the enhancement at intermediate p_T arises due to recombination or radial flow,

we examine the baryon-to-meson ratios involving similar masses, such as p/ϕ and p/K^{*0} using EPOS4 with and without UrQMD and compared them with ALICE measurements as shown in Fig. 7. However, the p/ϕ ratio from ALICE data shows a rather independent p_T up to 4 GeV/c, similar flat trend is seen by EPOS4 with UrQMD ON up to p_T (< 1.5 GeV/c). At high- p_T , both data and model results show similar decreasing trend for all particle species that suggests that a common fragmentation mechanism play important role, while model overestimates the data. Although EPOS4 with UrQMD ON describes the p/π ratio for stable hadrons, EPOS4 with UrQMD OFF fails to capture the exact enhancement trend in the intermediate p_T region. Furthermore, the results from EPOS4 with UrQMD OFF do not describe the measured ratios when one of the particles involved is a resonance. The p/K^{*0} ratio from ALICE measurements shows a slight decreasing trend, which is similarly supported by model results. This behavior is expected, as the K^{*0} spectral shape is modified due to

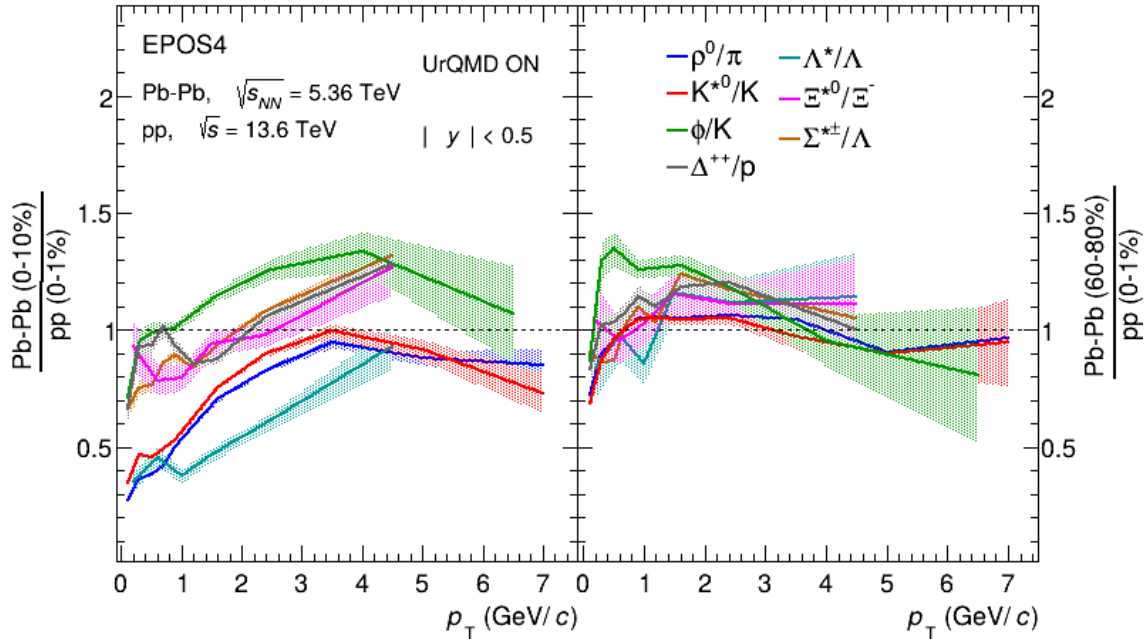


Fig. 5: The comparison of p_T -differential ratios ρ^0/π , K^{*0}/K , ϕ/K , Λ^*/Λ , Ξ^{*0}/Ξ^- and $\Sigma^{*\pm}/\Lambda$ in the central (0–10%, left) and peripheral (60–80%, right) Pb–Pb collisions at $\sqrt{s_{NN}} = 5.36$ TeV to the high multiplicity (0–1%) pp collisions at $\sqrt{s} = 13.6$ TeV with UrQMD. The bands in the measurements represent statistical uncertainty.

hadronic phase effects that dominate in the low p_T region. At high p_T , proton, K^{*0} and ϕ show similar decreasing trend. The EPOS4 describes the p/K^{*0} ratio qualitatively similar to the data but underestimated at low- p_T . This indicating that although protons, K^{*0} , ϕ have different quark content, the mass of hadrons and the hadronic phase effect on short-lived resonances that play important role in the determination of the spectral shape.

3.3 Average transverse momentum ($\langle p_T \rangle$)

The $\langle p_T \rangle$ of various hadronic resonances as a function of average charged particle multiplicity is shown in Fig. 6 for mid-rapidity in pp collisions at $\sqrt{s} = 13.6$ TeV and in Pb–Pb collisions at $\sqrt{s_{NN}} = 5.36$ TeV. These calculations are obtained using EPOS4 with and without UrQMD hadronic afterburner. The results are also compared with the measurements from ALICE Collaboration for pp collisions at $\sqrt{s} = 13$ TeV, 2.76 TeV [3, 4, 5] and Pb–Pb collisions at $\sqrt{s_{NN}} = 5.02$ TeV, 2.76 TeV [3, 8, 42], when available. The $\langle p_T \rangle$ increases with increasing charged particle multiplicity and mass of hadron species. The steeper rise in $\langle p_T \rangle$ for pp collisions compared to Pb–Pb collisions is well reproduced by the EPOS4, showing similar behavior to that observed in the data. The EPOS4 model gener-

ally reproduces the observed $\langle p_T \rangle$ trends in Pb–Pb collisions, demonstrating good agreement with experimental data across various centralities. In contrast, for pp collisions, EPOS4 tends to slightly underestimate the $\langle p_T \rangle$ values, particularly at higher multiplicities. Activating the hadronic cascade (UrQMD ON) typically leads to an increase in $\langle p_T \rangle$, improving the model’s consistency with measured data. This enhancement reflects the significant role of hadronic rescattering in modifying the p_T spectra during the later stages of collision evolution.

The $\langle p_T \rangle$ values for short-lived resonances such as ρ^0 , K^{*0} show significant changes between with and without UrQMD for Pb–Pb collision, whereas the effect is less pronounced for pp collisions. For the ϕ -meson, the difference in $\langle p_T \rangle$ between the two cases (with and without UrQMD) is smaller because its decay daughters interact less with the hadronic medium due to its longer lifetime. The change in $\langle p_T \rangle$ can be attributed to modifications in the spectral shape, as shown in Fig. 1 and Fig. 2. For short-lived resonances, their decay daughters undergo substantial hadronic interactions in the hadronic phase, leading to pronounced modifications. This effect is strongest in central Pb–Pb collisions and decreases with lower multiplicity, consistent with the shorter hadronic phase lifetimes discussed later in Sec-

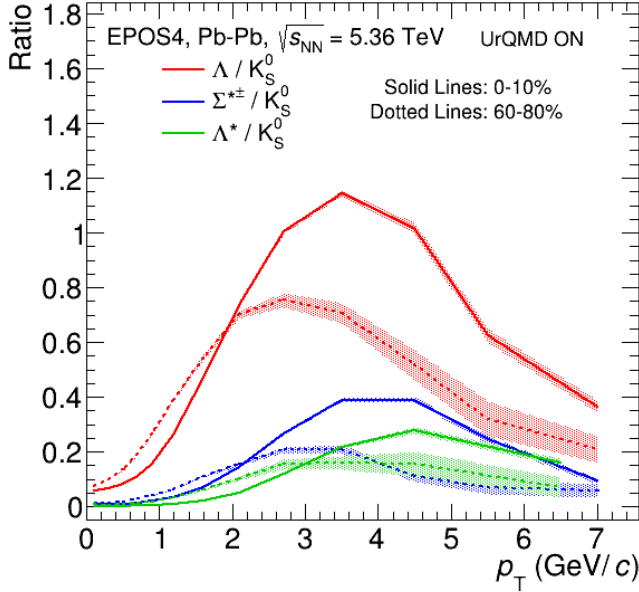


Fig. 6: The p_T -differential ratios Λ/K_S^0 , $\Sigma^{*\pm}/K_S^0$, and Λ^*/K_S^0 in central (0–10%, solid lines) and peripheral (60–80%, dotted lines) Pb–Pb collisions at $\sqrt{s_{NN}} = 5.36$ TeV, simulated using EPOS4 with UrQMD. The shaded bands represent statistical uncertainties in the measurements.

tion 3.5. For baryonic resonances such as $\Sigma^{*\pm}$, Λ^* , and Ξ^{*0} , no significant change in $\langle p_T \rangle$ is observed for small systems (up to $dN_{ch}/d\eta \sim 35$). However, in Pb–Pb collisions, both the spectral shape and the $\langle p_T \rangle$ values exhibit significant modifications due to the extended hadronic phase. It is observed that the particles with similar masses, such as the proton and the ϕ -meson, show comparable $\langle p_T \rangle$ values in central Pb–Pb collisions, as reported by ALICE measurements [13, 38]. This observation aligns with expectations from hydrodynamical models, which predict that $\langle p_T \rangle$ primarily depends on particle mass in such collisions. The EPOS4 model calculations also support this trend.

The $\langle p_T \rangle$ value of the proton shows a slight difference between simulations with and without UrQMD, suggesting that feed-down contributions from resonance decays are necessary to accurately describe the proton p_T spectrum. In contrast, the ϕ -meson momentum spectrum is negligibly affected by the hadronic phase due to its longer lifetime and lower interaction cross-section with the hadronic medium (In Fig. 7, p_T -differential p/ϕ from EPOS4 shows a flat behavior at low p_T as seen in the data and overestimates after $p_T > 2$ GeV/c).

The $\langle p_T \rangle$ as a function of reduced mass (Mass/N_q), where the mass of hadron is scaled by the number

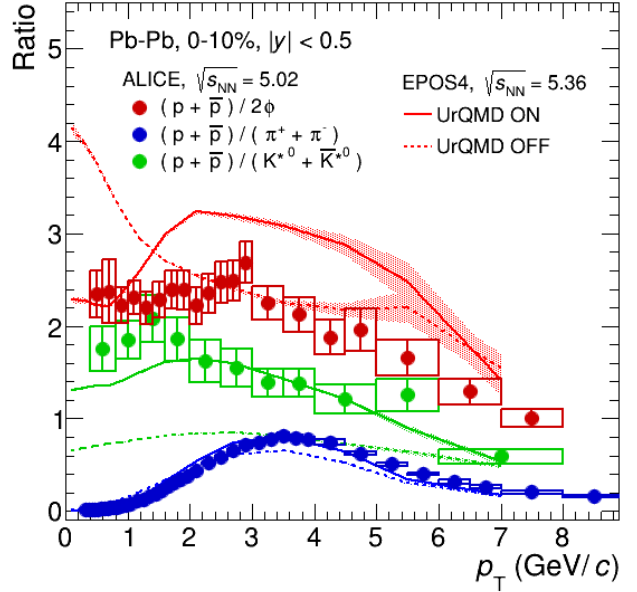


Fig. 7: The p_T -differential ratios p/ϕ , p/π and p/K^{*0} in the central Pb–Pb collisions with ALICE at $\sqrt{s_{NN}} = 5.02$ TeV (markers) and using EPOS4 model with UrQMD (solid lines) and without UrQMD (dotted lines) at $\sqrt{s_{NN}} = 5.36$ TeV. The bars and boxes in the ALICE measurements represent statistical and systematic uncertainties, respectively. The shaded area in the model calculations represent statistical uncertainty.

of valence quarks, is calculated for various light-flavor hadrons, including resonances for high multiplicity (0–1%) pp collisions at $\sqrt{s} = 13.6$ TeV and central (0–10%) Pb–Pb collisions at $\sqrt{s_{NN}} = 5.36$ TeV using the EPOS4 model, both with and without UrQMD, as shown in Fig. 9. The $\langle p_T \rangle$ follows a linear trend with increasing mass. Baryons and mesons group separately and exhibit parallel trends to each other. It is observed that stable mesons (red markers) and mesonic resonances (green markers) generally follow a linear trend, aligning closely with the linear fit function represented by the green line for both UrQMD ON and OFF. However, the ρ^0 , K^{*0} , $K^{*\pm}$, and Δ^{++} resonances slightly deviate from the linear trend, with different values observed between UrQMD ON and OFF. This deviation is expected due to the finite hadronic phase in high-multiplicity (0–1%) pp collisions, which leads to the modification of the spectral shape of short-lived resonances. Similarly, the observed deviation from the linear function increases for Pb–Pb collisions compared to pp collisions. Hadronic resonances like ρ^0 , K^{*0} , $K^{*\pm}$, Δ^{++} , Σ^\pm , and Λ^* show significant deviations from the expected linear trend due to larger system size.

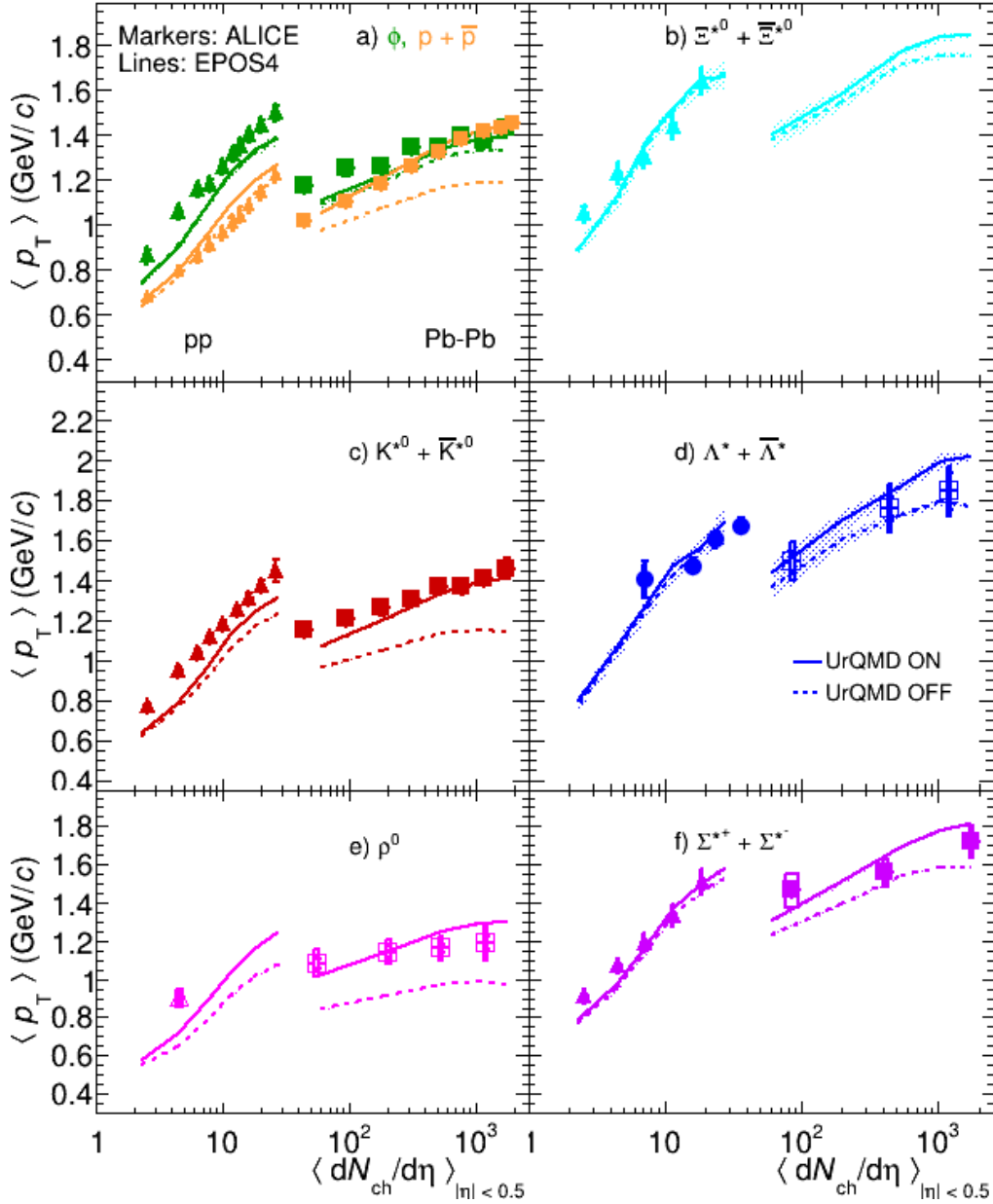


Fig. 8: Average transverse momentum of protons, mesonic resonances (ρ^0 , K^{*0} , and ϕ) and baryonic resonances ($\Sigma^{*\pm}$, Λ^* , Ξ^{*0}) as a function of charged particle multiplicity density at intermediate-rapidity. Markers indicate ALICE measurements in pp system at $\sqrt{s} = 2.76$ TeV (open triangles) [5] and $\sqrt{s} = 13$ TeV (solid triangles) [3, 4, 41], in p-Pb system at $\sqrt{s_{NN}} = 5.02$ TeV (solid circles) [6], and in Pb-Pb system at $\sqrt{s_{NN}} = 2.76$ TeV (open squares) [5, 12] and $\sqrt{s_{NN}} = 5.02$ TeV (solid squares) [8, 13, 38]. The lines represent EPOS4 predictions for pp collisions at $\sqrt{s} = 13.6$ TeV and for Pb-Pb collisions at $\sqrt{s_{NN}} = 5.36$ TeV with UrQMD (solid lines) and without UrQMD (dotted lines). The statistical and systematic uncertainties in the ALICE data are represented by bars and boxes, respectively while the statistical uncertainty in the model measurements are represented by bands.

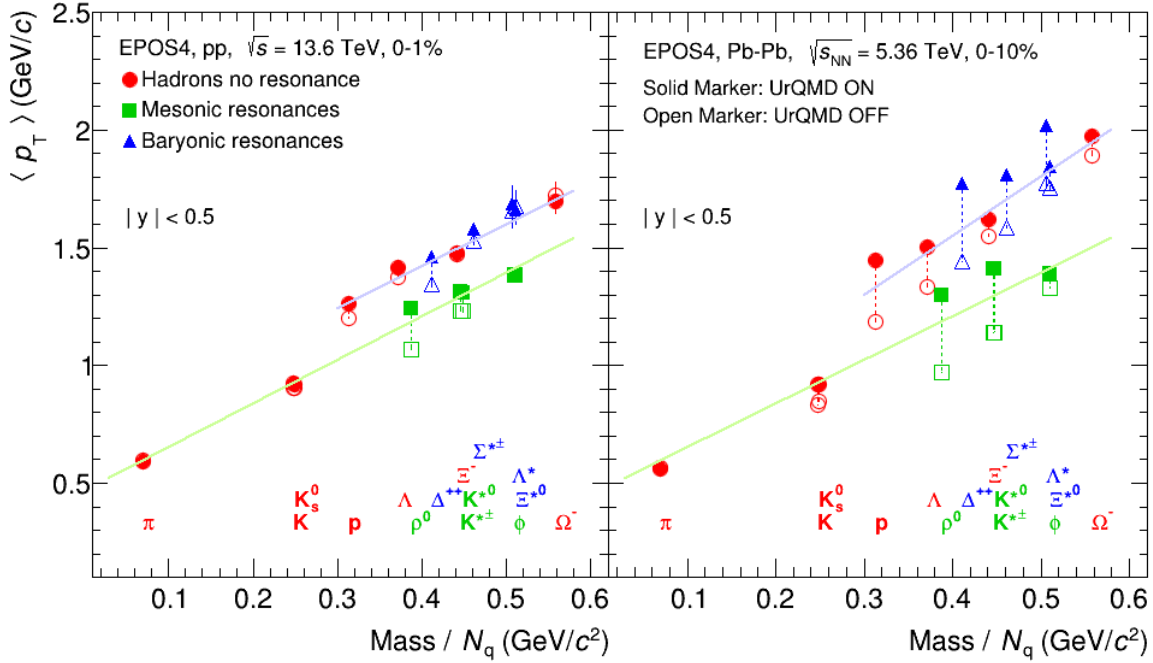


Fig. 9: The average transverse momentum of hadrons in the mid-rapidity region plotted as a function of the hadron mass, scaled by the number of valence quarks, in high multiplicity (0-1%) pp collisions at $\sqrt{s} = 13.6$ TeV (left panel) and in central (0-10%) Pb-Pb collisions at $\sqrt{s_{NN}} = 5.36$ TeV (right panel) using the EPOS4 model with UrQMD (solid markers) and without UrQMD (open markers). The green and blue lines represent linear functions. The statistical uncertainty in the measurements is represented by bars.

The $\langle p_T \rangle$ value is larger for short-lived resonances when UrQMD is ON compared to when it is OFF for most central Pb-Pb collisions. This indicates that the rescattering effect leads to increases the $\langle p_T \rangle$ value. Additionally, for stable hadrons like the proton and Λ , the $\langle p_T \rangle$ values deviate from the linear trend and differ between the cases with UrQMD ON and OFF. This indicates that the spectral shape and $\langle p_T \rangle$ of protons and Λ are modified in the hadronic phase due to contributions from the decay of higher resonance states, as they are likely decay daughters.

3.4 Resonance to non-resonance yield ratios

Figure 10 presents the resonance-to-stable-hadron yield ratios as a function of charged-particle multiplicity ($dN_{ch}/d\eta$) at mid-rapidity for pp and Pb-Pb collisions at LHC energies. Recent measurements of the ρ^0/π and K^{*0}/K ratios show a decreasing trend with increasing multiplicity. These ratios have been investigated using the EPOS4 model, both with and without the UrQMD hadronic afterburner. A significant difference is observed between the model predictions with

and without UrQMD, with the difference being more pronounced in central Pb-Pb collisions compared to pp collisions. Furthermore, this difference is more significant for resonances with shorter lifetimes compared to those with longer lifetimes. The EPOS4 model, with the UrQMD hadronic afterburner enabled, successfully captures the features and qualitatively describes the behavior observed in the data. The K^{*0} and ϕ resonances are ideal candidates for these ratios because they have similar masses and contain strange quarks, while differing by lifetimes of an order of magnitude of 10. The ratios are chosen in such a way that the strangeness effect on the production yield is canceled out, allowing for a more direct comparison of resonance yields relative to stable hadrons. Suppression in the K^{*0}/K ratio suggests that the decay daughters of the resonance undergo rescattering processes in the hadronic phase, resulting in a modified final yield of the resonance compared to what was originally produced before chemical freeze-out. This suppression becomes more pronounced with increasing system size. The observed suppression in the K^{*0}/K ratio, compared to the ϕ/K ratio across small to large collision systems, supports the idea that the shorter lifetime

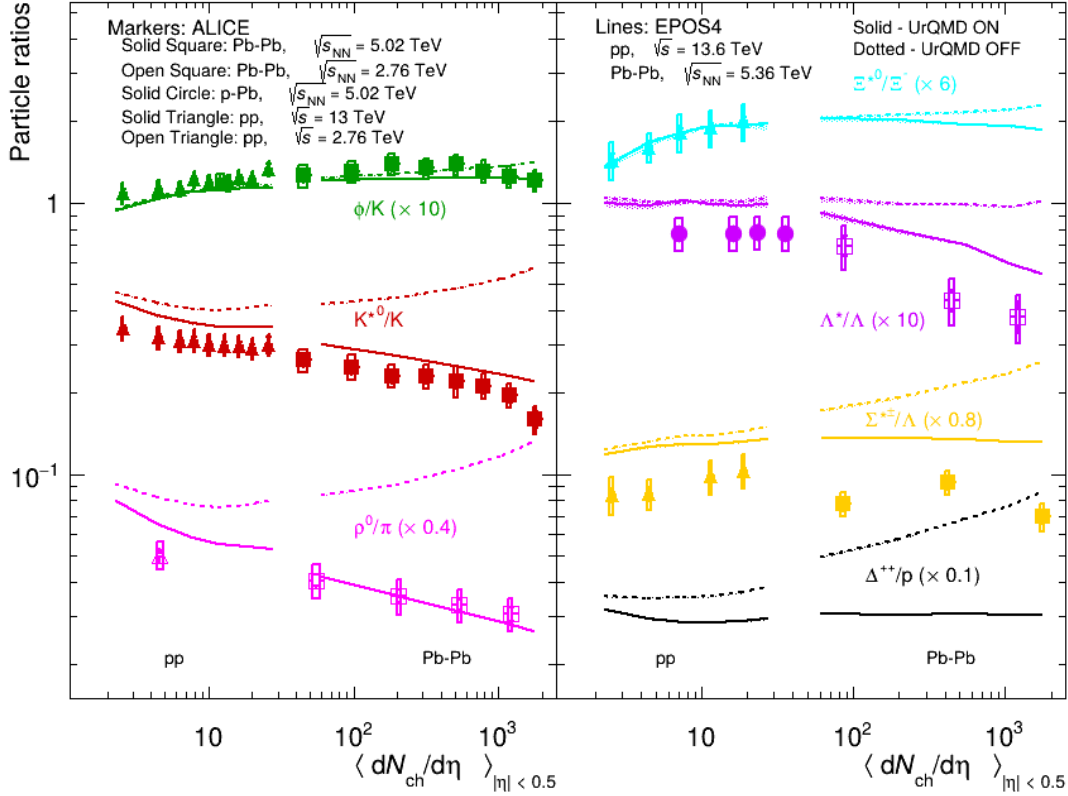


Fig. 10: Left panel shows the ratios of mesonic resonances to stable mesons yield while the right panel shows the ratios of baryonic resonances to stable baryons yield. Different markers represent ALICE results in pp collisions at $\sqrt{s_{NN}} = 13$ TeV (solid triangles) [3, 4] and $\sqrt{s_{NN}} = 2.76$ TeV (open triangles) [5], p-Pb collisions at $\sqrt{s_{NN}} = 5.02$ TeV (solid circles) [6], Pb-Pb collisions at $\sqrt{s_{NN}} = 2.76$ TeV (open squares) [5] and $\sqrt{s_{NN}} = 5.02$ TeV (solid squares) [7, 8]. The statistical and systematic uncertainties in the data are represented by bars and boxes, respectively. The lines represent predictions from EPOS4 in pp collisions at $\sqrt{s_{NN}} = 13.6$ TeV and in Pb-Pb collisions at $\sqrt{s_{NN}} = 5.36$ TeV with UrQMD (solid) and without UrQMD (dotted). The shaded area indicates the statistical uncertainty in the model calculations.

of the K^{*0} plays a significant role in modifying the resonance yield in the hadronic phase. Similarly, the short-lived ρ^0/π ratio also shows suppression with increasing multiplicity. Observations from both data and model results indicate that re-scattering effects dominate over regeneration in the hadronic phase for short-lived mesonic resonances.

Similarly, Fig. 10 (right) shows the ratios of baryonic resonances to stable hadrons as a function of $dN_{ch}/d\eta$ at mid-rapidity. The Ξ^{*0}/Ξ^- ratio increases with multiplicity, whereas the Λ^*/Λ and Σ^*/Λ ratios show no significant change with multiplicity in pp collisions. In the Pb-Pb collisions, the Λ^*/Λ ratio decreases with increasing multiplicity, while the Ξ^{*0}/Ξ^- and $\Sigma^{*\pm}/\Lambda$ ratios remain largely unaffected, despite the fact that the $\Sigma^{*\pm}$ resonance has a shorter lifetime (5.0–5.5 fm/c) compared

to the Λ^* (12.6 fm/c). This behavior may be attributed to the fact that the decay daughters of these resonances undergo regeneration and rescattering through (pseudo)-elastic interactions in the hadronic phase. In the case of $\Sigma^{*\pm}$, the regeneration and rescattering effects are expected to cancel each other out, resulting in minimal changes in yield with increasing system size. In contrast, the decreasing trend of the Λ^*/Λ ratio with multiplicity is primarily driven by rescattering effects. However, recent studies reported in Ref. [17] suggest that the mean free path of resonances also plays a significant role in modifying the final yield. The Ξ^{*0}/Ξ^- also show a weak dependence with multiplicity due to larger lifetime compared to Λ^* . For Δ^{++} resonance, it is observed that Δ^{++}/p shows flat behavior with multiplicity for Pb-Pb collisions whereas the same ratios exhibit a decreasing

trend for pp collisions. Based on experimental data and model calculations, baryonic resonances exhibit distinct behaviors in pp and Pb–Pb collisions. This indicates that the modification of final resonance yields in the hadronic phase is not solely determined by the resonance lifetime. Other factors, such as the mean free path of resonances, the duration of the hadronic phase, the cross-section of the decay products, and the chemical freeze-out temperature, also play a significant role.

3.5 Lifetime of hadronic phase

The suppression of short-lived resonances is seen in both ALICE data and model results from EPOS4 with UrQMD. The suppression in the resonance to stable hadron yield is likely caused by the rescattering of decay products of resonances in the hadronic phase. These ratios act as useful tools for estimating the timespan between chemical and kinetic freeze-outs using the exponential decay law, under the following assumptions:

- i) Negligible regeneration effects.
- ii) Simultaneous freeze-out for all particle species. The relation is given by:

$$[h^*/h]_{kinetic} = [h^*/h]_{chemical} \times e^{-\tau/\tau_{h^*}} \quad (1)$$

where $[h^*/h]_{kinetic}$ denotes the yield ratio of resonance to stable hadron at kinetic freeze-out, τ_{h^*} is the lifetime of the resonance particle in its rest frame, and τ is timespan of the hadronic phase. Under these assumptions, all resonance particles decaying before kinetic freeze-out are lost due to rescattering of their decay daughters in the hadronic gas, with no regeneration of resonances through elastic scattering. Thus, the estimated time duration is considered as the lower limit for the timespan between chemical and kinetic freeze-outs.

For this calculation, it is further assumed that no hadronic phase forms in pp collisions due to the small system size. Therefore, the yield ratio in minimum bias pp collisions is used as a proxy for $[h^*/h]_{chemical}$. A Lorentz boost factor is also applied in the calculation of τ because the lifetime of resonance is dilated when transitioning from the rest frame of the resonance to the laboratory reference frame. This factor is approximated as $\sqrt{1 + (\langle p_T \rangle / mc)^2}$, where $\langle p_T \rangle$ is the average transverse momentum and m is the rest mass of the resonance particle. The methodology used to estimate τ is the same as discussed in Ref. [7]. The results for the estimated duration of the hadronic phase (τ) as a function of $\langle dN_{ch}/d\eta \rangle^{1/3}$ from ALICE measurements and EPOS4 with UrQMD using resonances (ρ^0 , K^{*0} and Λ^*) at LHC energies for pp and Pb–Pb collisions, are shown in Fig. 11. An increasing trend in the lifetime of hadronic

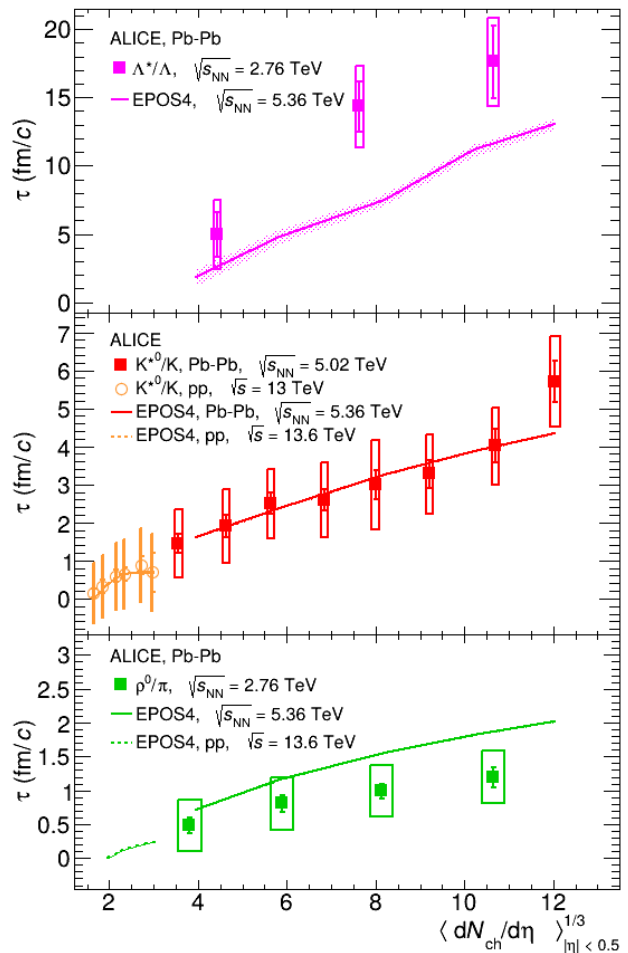


Fig. 11: Lower limit on the lifetime of the hadronic phase between chemical and kinetic freeze-outs in Pb–Pb collisions across different V0M multiplicity classes, obtained from yield ratios: Λ^*/Λ at $\sqrt{s_{NN}} = 2.76$ TeV (magenta markers) [12], K^{*0}/K at $\sqrt{s_{NN}} = 5.02$ TeV (red markers) [7], and ρ^0/π at $\sqrt{s_{NN}} = 2.76$ TeV (green markers) [5]. EPOS4 predictions for Pb–Pb collisions at $\sqrt{s_{NN}} = 5.36$ TeV are shown as lines, with shaded areas representing statistical uncertainties. Statistical and systematic uncertainties in the ALICE data are depicted by bars and boxes, respectively. The figure also includes ALICE measurements of K^{*0}/K in pp collisions at $\sqrt{s} = 13$ TeV (orange markers) [3] and EPOS4 predictions for pp at $\sqrt{s} = 13.6$ TeV (orange line), highlighting the system size dependence of the hadronic phase lifetime.

phase is observed for these resonances in both data and model, corresponding to the decreasing yield ratios (as shown in Fig. 10) as a function of system size. This trend is expected, as a larger system size at a fixed chemical freeze-out leads to a decrease in the kinetic freeze-out temperature, thereby a longer timespan exists between chemical and kinetic freeze-outs. This pattern is consistent with the simultaneous blast-wave fits of the identified particle p_T distributions [38]. The timespan of the hadronic phase calculated from the ρ^0/π , K^{*0}/K ratios, are lower than that from the Λ^*/Λ ratio. The model predictions for estimation of τ using the Λ^*/Λ ratios underestimate the data, whereas ρ^0/π overestimate the data. Although the experimental data and model predictions are obtained at slightly different energies, the comparison reveals only minor differences. Since particle production is primarily driven by charged-particle multiplicity, the dependence on collision energy is expected to be weak or negligible. However, the model predictions for K^{*0}/K ratio are in good agreement with the data. Contrary to the expectation of a common hadronic phase duration for all resonances, different values are found for the ρ^0 , K^{*0} , and Λ^* yields, with longer-lived resonances showing longer timescales. The observed different values in the time duration of the hadronic phase across different species may be attributed to additional factors beyond rescattering, which also contribute to the final modification of resonance yields. These factors are not accounted for in the simple exponential decay model, as described in Eq. 1. If regeneration is significant, the estimated duration from the yield ratios represents the timescale between delayed resonance production (caused by regeneration) and kinetic freeze-out. This duration reflects a lower limit for the actual hadronic-phase duration. To find the exact duration, the delay from regeneration needs to be added to this estimate. Recently hydrodynamics based SMASH model calculation suggest that mean free path of resonances also play an important role in the final yield of resonances Ref. [17]. Similar studies in particularly at high multiplicity pp collisions also play huge interest for better understanding of the microscopic origin of resonance suppression. The EPOS4 model results for K^{*0} with UrQMD in high-multiplicity pp collisions also show a nonzero hadronic phase duration, approximately matching the value in peripheral Pb–Pb collisions, thus highlighting the system size dependence of the hadronic phase lifetime, as shown in Fig. 11.

3.6 Strangeness enhancement

The relative yield ratios of various hadrons to pions serve as key observable to understand the origin of strangeness

production and the hadronization mechanism. Fig. 12 shows the yield ratios of protons, K_S^0 and multi-strange baryons (left), along with hadronic resonances (right), normalized to pions as a function of charged-particle multiplicity for pp to Pb–Pb collisions at LHC energies. The results from EPOS4 with and without UrQMD are represented by solid and dotted lines, respectively, and are compared with available measurements from the ALICE Collaboration [3, 4, 8, 12, 38, 39, 41, 43, 44]. The yield ratios exhibit a smooth evolution with multiplicity from pp to Pb–Pb collisions, whereas the $\langle p_T \rangle$ shows a discontinuous pattern with multiplicity, as seen in Fig. 8. This behavior can be understood as different saturation effects with multiplicity is expected for pp and Pb–Pb collisions. The saturation scale increases with multiplicity for pp collisions, whereas in Pb–Pb collisions, the saturation scale shows the more modest increase, as discussed in Ref. [22].

The observed enhancement in the production rates of strange hadrons relative to pions is primarily driven by the strange quark content of the hadrons rather than their mass. This effect appears more pronounced for heavier baryons containing strange quarks in pp collisions. For Pb–Pb collisions, the ratios attain a saturation trend for hadrons that contain strange quark at higher multiplicities. This behavior indicates that their production reaches a chemical equilibrium in central Pb–Pb collisions. The saturation reflects the system reach thermalized environment, where the production of strange and multi-strange hadrons becomes independent of further increases in multiplicity for central heavy-ion collisions at LHC energies. The EPOS4 model incorporates the micro canonical ensemble (MCE) framework reproduces the observed behavior in experimental data. However, when system gets very small, one gets reduction of heavy particle production due to micro canonical treatment of strange particle production which imposes constraints on energy and flavor conservation. This effect becomes more pronounced with increasing particle mass and is observed most significantly for Ω and Ξ baryons in pp collisions. The model results show a small difference with and without UrQMD tune for multi-strange hadrons for Pb–Pb collisions, whereas there is no significant difference for pp collisions.

Further, the same ratios to pion for hadronic resonances that content strange quarks of short-lived resonances (ρ, K^{*0} and Λ^*) show suppression behavior in central Pb–Pb collisions. The results with and without UrQMD show significantly different behavior. This indicates rescattering effect is dominant over strangeness enhancement. The ϕ -meson shows a weak enhancement trend, except in the most central Pb–Pb collisions, where

the measurements reveal a decreasing trend. A similar behavior is observed in the results with UrQMD. Future measurements will provide further constraints to understand this behavior.

The yield ratios of protons to pions show a decreasing trend at the highest multiplicities in Pb–Pb collisions, with a similar behavior observed in both data and EPOS4 model predictions using UrQMD, although the model results overestimate the measurements. This suppression is attributed to baryon-antibaryon annihilation at large multiplicities, which reduces the proton yield.

However, the effects of baryon-antibaryon annihilation appear less pronounced for strange baryons such as the Λ , Ξ^- and Ω^- at high multiplicities in Pb–Pb collisions. To further understand the production of non-strange and strange baryons in Pb–Pb collisions, the yield ratios of Λ , Ξ^- and Ω^- to protons, as a function of charged-particle multiplicity and normalized to the values measured in inelastic pp collisions, have been calculated using EPOS4 with UrQMD predictions. The results are shown in Fig. 13. The ratios for Δ^{++} show a flat behavior with multiplicity for Pb–Pb collisions, as expected, since Δ^{++} has no strange content and no hadronic phase effects are observed, as discussed in Fig. 10. Similarly, the same ratios for Λ , Ξ^- and Ω^- increase with multiplicity, with the rate of enhancement rising according to the strange quark content of the hadrons. This behavior can be understood as a competitive interplay between strangeness production and baryon-antibaryon annihilation processes, which influence multi-strange baryon production in the high-multiplicity environment of Pb–Pb collisions at LHC energies. The stepper rise in the slope of the ratios is observed in pp collisions. Future experimental measurements of these ratios at the LHC will provide deeper insights, helping to distinguish between the effects of strangeness production and baryon-antibaryon annihilation.

This observation suggests that the net suppression in the most central Pb–Pb collisions depends on the modification of hadron yields due to combined contributions from various processes, such as strangeness production, baryon-antibaryon annihilation, and hadronic phase effects.

4 Summary

In this work, we present the study of various hadronic resonances to explore production dynamics and their interactions, along with other stable non-strange and strange hadrons at midrapidity for pp and Pb–Pb collisions at $\sqrt{s} = 13.6$ TeV and $\sqrt{s_{NN}} = 5.36$ TeV, using

the EPOS4 model. The results are new findings with the latest EPOS model, extending such studies for first time to high-multiplicity pp collisions and the highest energies for Pb–Pb collisions at the LHC. The EPOS4 with UrQMD as the hadronic afterburner, is well suited for describing experimental measurement of resonances in high-energy collisions. The EPOS4 calculations in the yield ratios of resonances to ground-state particles successfully capture the qualitative trend of these ratios with varying system sizes from pp to Pb–Pb collisions. The ratios for shorter-lived resonances (ρ^0 , K^{*0} , Λ^*) are suppressed, while Ξ^{*0} exhibits a weak suppression, and $\Sigma^{*\pm}$ and Δ^{++} remain unaffected with multiplicity in large collision systems. This suppression is not seen in the ϕ meson due to its longer lifetime compared to other resonances.

The precision studies of heavier baryonic resonance (Ξ^{*0} , $\Sigma^{*\pm}$) and predictions for Δ^{++} await confirmation through future measurements at the LHC. The calculations for ρ/π , K^{*0}/K ratios show a decreasing trend in pp collisions. This tends to be consistent with the similar picture that is seen in the measured K^{*0}/K ratio for pp collisions by the ALICE Collaboration. The lower limit of time duration (τ) of the hadronic phase are estimated using the yield ratios of ρ/π , K^{*0}/K and Λ^*/Λ , and it increases with the system size. A nonzero time duration ($\sim 0.5 - 1$ fm/ c) is found in high-multiplicity pp collisions. The suppression in these ratios is due to the modification of the yields in the hadronic phase due to rescattering processes, it is mainly governed at low p_T regions and the effect is more significant for short-lived resonances.

Enabling UrQMD improves the description of the $\langle p_T \rangle$ values for various hadronic resonances and protons. In central Pb–Pb collisions, the mass ordering of $\langle p_T \rangle$ for particles with similar masses (e.g., p and ϕ) aligns with hydrodynamic predictions, but this ordering breaks down in peripheral Pb–Pb and pp collisions. The $\langle p_T \rangle$ as a function of reduced mass (scaled by the number of valence quarks) shows a linear increasing trend. The baryons and mesons form distinct groups that are parallel to each other. For short-lived resonances such as ρ^0 and K^{*0} , deviations from the linear trend are observed in high-multiplicity pp collisions and more significant for the central Pb–Pb collisions. This indicates that rescattering effect increases the $\langle p_T \rangle$ values for short-lived resonances. Moreover, for stable hadrons like proton and Λ , the $\langle p_T \rangle$ values differ significantly with and without UrQMD, particularly in central Pb–Pb collisions, suggesting that their spectral shapes and $\langle p_T \rangle$ values are influenced by the decays of higher-mass resonances.

The baryon-to-meson ratios in central and peripheral

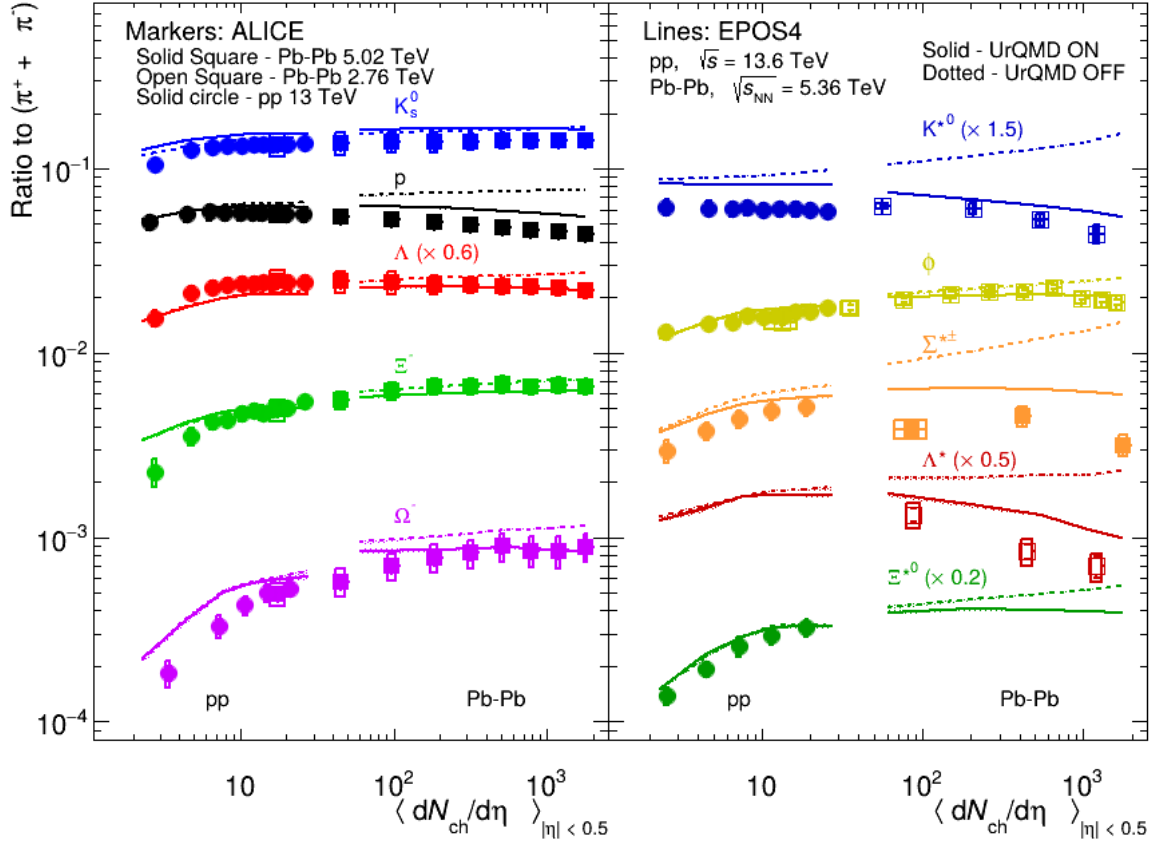


Fig. 12: Left panel shows the ratios of proton, strange and multi-strange hadrons while the right panel shows the ratios of hadronic resonances, normalized to pions yield. Different markers represent ALICE results in pp collisions at $\sqrt{s_{NN}} = 13$ TeV (solid circles) [3, 4, 39, 41, 43] and Pb–Pb collisions at $\sqrt{s_{NN}} = 2.76$ TeV (open squares) [12, 44] and $\sqrt{s_{NN}} = 5.02$ TeV (solid squares) [8, 38]. The statistical and systematic uncertainties in the data are represented by bars and boxes, respectively. The lines represent predictions from EPOS4 in pp collisions at $\sqrt{s_{NN}} = 13.6$ TeV and in Pb–Pb collisions at $\sqrt{s_{NN}} = 5.36$ TeV with UrQMD (solid) and without UrQMD (dotted). The shaded area indicates the statistical uncertainty in the model calculations.

Pb–Pb collisions at $\sqrt{s_{NN}} = 5.36$ TeV have been measured. This suggests that the radial flow plays a dominant role in enhancing the Λ^*/K_S^0 , and $\Sigma^{*\pm}/K_S^0$ ratios in the intermediate p_T region. Additionally, the p/ϕ and p/K^{*0} ratios remain nearly flat in the intermediate p_T . At high p_T , all the ratios exhibit the similar decreasing trend, suggesting the common fragmentation process influencing their production.

To understand the microscopic origin of the strangeness production, the strange and multi-strange hadrons along with resonances are investigated. The relative yield ratios of hadrons to pions smoothly increase with multiplicity, with the rate of increase depending on the strange quark content of the hadrons. However, the ratios attain the saturation trend at higher multiplicities

(> 100), consistent with predictions for the strangeness productions in the micro canonical treatment at higher densities.

The p/π ratios exhibit the decreasing trend with increasing multiplicity, the behavior that becomes more pronounced at higher multiplicities for Pb–Pb collisions. This trend is observed in both experimental data and model predictions. The suppression at higher densities is primarily driven by baryon-antibaryon annihilation for non-strange hadrons (p) whereas this effect is less pronounced for heavier multi-strange baryons (Λ , Ω , and Ξ).

The p_T spectra and yields of various hadrons, including resonances, are influenced by processes such as rescattering, regeneration, annihilation, and radial flow. There-

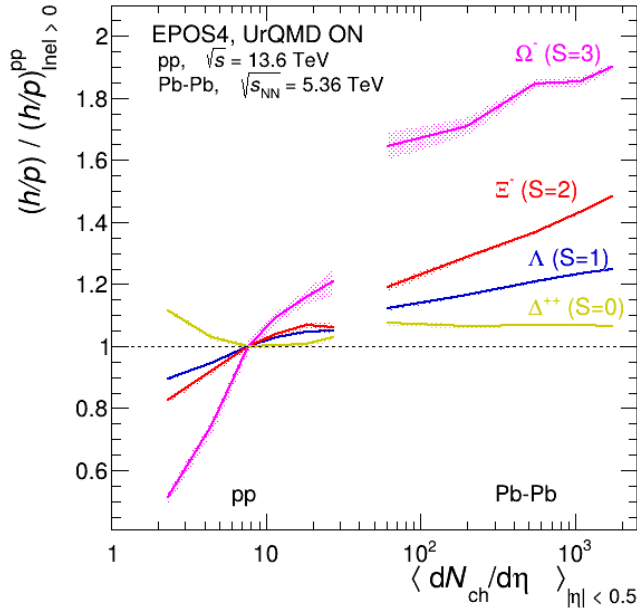


Fig. 13: Particle yield ratios to proton, normalized to the values measured inelastic pp collisions, as predicted by the EPOS4 model with UrQMD. The results are shown for Δ^{++} and multi-strange baryons in Pb–Pb collisions at $\sqrt{s_{NN}} = 5.36$ TeV and in pp collisions at $\sqrt{s} = 13.6$ TeV. The bands in the measurements represent statistical uncertainty.

fore, the comprehensive understanding of the hadronic phase, even in small collision systems, is essential for accurately interpreting observables that reveal the underlying production dynamics. Future measurements of resonance such as the Δ^{++} , $f_0(980)$, $\Lambda(1405)$, $N(1535)$, $K1(1270)$, along with differential studies of the resonance flow and association with jets, will further probe hadronic phase that created in high energy collisions at LHC energies.

5 Acknowledgement

We sincerely thank K. Werner for his invaluable contributions through insightful discussions and for providing critical technical details related to the EPOS4 model. The authors at University of Jammu gratefully acknowledge the Department of Science and Technology (DST), Government of India, for their financial support in doing this work. We also extend our gratitude to the CERN Grid computing centre for providing the computational resources required for this work.

References

- [1] J. W. Harris and B. Muller, *Ann. Rev. Nucl. Part. Sci.* **46**, 71 (1996), [hep-ph/9602235](#).
- [2] S. Acharya et al. (ALICE), *Eur. Phys. J. C* **84**, 813 (2024), [2211.04384](#).
- [3] S. Acharya et al. (ALICE), *Phys. Lett. B* **807**, 135501 (2020), [1910.14397](#).
- [4] S. Acharya et al. (ALICE), *JHEP* **05**, 317 (2024), [2308.16116](#).
- [5] S. Acharya et al. (ALICE), *Phys. Rev. C* **99**, 064901 (2019), [1805.04365](#).
- [6] S. Acharya et al. (ALICE), *Eur. Phys. J. C* **80**, 160 (2020), [1909.00486](#).
- [7] S. Acharya et al. (ALICE), *Phys. Lett. B* **802**, 135225 (2020), [1910.14419](#).
- [8] S. Acharya et al. (ALICE), *Eur. Phys. J. C* **83**, 351 (2023), [2205.13998](#).
- [9] B. I. Abelev et al. (STAR), *Phys. Rev. Lett.* **97**, 132301 (2006), [nucl-ex/0604019](#).
- [10] J. Adams et al. (STAR), *Phys. Rev. C* **71**, 064902 (2005), [nucl-ex/0412019](#).
- [11] L. Gaudichet (STAR), *J. Phys. G* **30**, S549 (2004), [nucl-ex/0307013](#).
- [12] S. Acharya et al. (ALICE), *Phys. Rev. C* **99**, 024905 (2019), [1805.04361](#).
- [13] S. Acharya et al. (ALICE), *Phys. Rev. C* **106**, 034907 (2022), [2106.13113](#).
- [14] S. Acharya et al. (ALICE), *Phys. Rev. C* **107**, 055201 (2023), [2110.10042](#).
- [15] Z.-W. Lin, C. M. Ko, B.-A. Li, B. Zhang, and S. Pal, *Phys. Rev. C* **72**, 064901 (2005), [nucl-th/0411110](#).
- [16] A. Motornenko, V. Vovchenko, C. Greiner, and H. Stoecker, *Phys. Rev. C* **102**, 024909 (2020), [1908.11730](#).
- [17] D. Oliinychenko and C. Shen, arXiv preprint (2021), [hep-ph], [2105.07539](#).
- [18] A. G. Knospe, C. Markert, K. Werner, J. Steinheimer, and M. Bleicher, *Phys. Rev. C* **104**, 054907 (2021), [2102.06797](#).

-
- [19] A. G. Knospe, C. Markert, K. Werner, J. Steinheimer, and M. Bleicher, Phys. Rev. C **93**, 014911 (2016), [1509.07895](#).
- [20] B. B. Abelev et al. (ALICE), Int. J. Mod. Phys. A **29**, 1430044 (2014), [1402.4476](#).
- [21] M. Tanabashi et al. (Particle Data Group), Phys. Rev. D **98**, 030001 (2018).
- [22] K. Werner, Phys. Rev. C **109**, 014910 (2024), [2306.10277](#).
- [23] V. N. Gribov, Zh. Eksp. Teor. Fiz. **53**, 654 (1967).
- [24] V. N. Gribov, Sov. Phys. JETP **29**, 483 (1969).
- [25] V. N. Gribov and L. N. Lipatov, Sov. J. Nucl. Phys. **15**, 438 (1972).
- [26] V. A. Abramovsky, V. N. Gribov, and O. V. Kancheli, Yad. Fiz. **18**, 595 (1973).
- [27] G. Altarelli and G. Parisi, Nucl. Phys. B **126**, 298 (1977).
- [28] Y. L. Dokshitzer, Sov. Phys. JETP **46**, 641 (1977).
- [29] L. V. Gribov, E. M. Levin, and M. G. Ryskin, Phys. Rept. **100**, 1 (1983).
- [30] L. D. McLerran and R. Venugopalan, Phys. Rev. D **49**, 3352 (1994), [hep-ph/9311205](#).
- [31] L. D. McLerran and R. Venugopalan, Phys. Rev. D **49**, 2233 (1994), [hep-ph/9309289](#).
- [32] A. Kovner, L. D. McLerran, and H. Weigert, Phys. Rev. D **52**, 3809 (1995), [hep-ph/9505320](#).
- [33] Y. V. Kovchegov, Phys. Rev. D **54**, 5463 (1996), [hep-ph/9605446](#).
- [34] T. Pierog, I. Karpenko, J. M. Katzy, E. Yatsenko, and K. Werner, Phys. Rev. C **92**, 034906 (2015), [1306.0121](#).
- [35] K. Werner, Phys. Rev. Lett. **98**, 152301 (2007), [0704.1270](#).
- [36] K. Werner, I. Karpenko, T. Pierog, M. Bleicher, and K. Mikhailov, Phys. Rev. C **82**, 044904 (2010), [1004.0805](#).
- [37] K. Werner, B. Guiot, I. Karpenko, and T. Pierog, Phys. Rev. C **89**, 064903 (2014), [1312.1233](#).
- [38] S. Acharya et al. (ALICE), Phys. Rev. C **101**, 044907 (2020), [1910.07678](#).
- [39] S. Acharya et al. (ALICE), Eur. Phys. J. C **81**, 256 (2021), [2005.11120](#).
- [40] R. J. Fries, B. Muller, C. Nonaka, and S. A. Bass, Phys. Rev. Lett. **90**, 202303 (2003), [nucl-th/0301087](#).
- [41] S. Acharya et al. (ALICE), Eur. Phys. J. C **80**, 693 (2020), [2003.02394](#).
- [42] J. Adam et al. (ALICE), Eur. Phys. J. C **76**, 245 (2016), [1601.07868](#).
- [43] S. Acharya et al. (ALICE), Eur. Phys. J. C **80**, 167 (2020), [1908.01861](#).
- [44] B. B. Abelev et al. (ALICE), Phys. Rev. C **91**, 024609 (2015), [1404.0495](#).